Improved Uniformity in Glass TSV Filling by Asymmetric Dwell Pulsed Potential Deposition

Youjung Kim[1,2,*], Eun Soo Shim[1,3,*], Ji Young Park[1,2], Matthew S. Weimer[4], Sara Harris[4], David Raciti[1], Bongyoung Yoo[2], Jae-Hong Lim[3], Yong-Ho Choa[2], Thomas P. Moffat[1] and Daniel Josell[1]

1. Materials Science and Engineering Division, Materials Measurement Laboratory, National Institute of Standards and Technology, 100 Bureau Drive, Gaithersburg, MD 20899.

2. Department of Materials Science and Chemical Engineering, Hanyang University, Ansan-si 15588, Republic of Korea.

3. Department of Materials Science and Engineering, Gachon University, Seongnam-si 13120, Republic of Korea.

4. Forge Nano, Inc., 12300 Grant St. #110, Thornton, CO 80241

*. The first two authors contributed equally to this work

ABSTRACT

Filling of through vias in glass interposers is explored using an acid copper sulfate electrolyte containing dilute chloride and a polyether suppressor additive. Cyclic voltammetry with a rotating disk electrode shows that suppression breakdown and hysteresis is associated with an S-shaped negative differential resistance (S-NDR). Feature filling experiments at potentials within the hysteretic potential range yield localized deposition that initiates and advances from the center of the through vias to enable void-free Cu filling. Challenges with filling uniformity across the interposer workpiece are addressed using an asymmetric pulsed potential approach to periodically reinforce active growth on the most recessed surface regions. The activation and

deposition potentials are selected based on voltammetry and the S-NDR filling mechanism while accounting for distributed ohmic losses due to uncompensated electrolyte and contact resistances.

INTRODUCTION

Advanced packaging is central to the future of microelectronics, and the ability to fabricate ever smaller, higher aspect interconnects will be required to enable further densification needed for higher performance and gains in functionality. The high conductivity of copper and the ability to robustly fill recessed features in patterned dielectric materials with copper by surfactant mediated electrodeposition account for its central role in interconnect circuitry. This includes building circuits for on-chip metallization[1-3] and through silicon vias for chip stacking[4-8], as well as fan out I/O and microvias[9-14] and through holes in printed circuit boards and ultra-thin glass interposers and advanced packaging[13-31]. Surfactant additives enable void-free metal filling of high aspect ratio recessed features by highly localized bottom-up filling or superconformal deposition. These processes have been applied most prominently to Cu due to its industrial significance. However, they have also been demonstrated for other metals including Ag[32], Au[33-34], Co[35-38] and Ni[39,40] using different electrolyte-additive combinations to generate the desired superconformal or bottom-up filling response. Of particular interest are electrolytes that contain dilute surfactant additives whose adsorption either accelerate or suppress the metal deposition reaction wherein local variations in rate arise from spatial nonuniform adsorbate coverage due to the impact of transport, area change, deactivation by burial and/or other phenomena.

For filling of large features whose dimensions approach that of the hydrodynamic boundary layer, e.g., through silicon vias (TSV) in wafer stacking applications, blind vias in printed

circuit boards or through hole vias (THV) in printed circuit boards, the additive and reactant gradients and transport conditions play an important role in the filling process. For dilute additive concentrations, diffusional transport within the electrolyte coupled with adsorbate burial in the growing deposit can create concentration gradients and variations in adsorbate coverage on the neighboring surfaces.[5-8,13,23,25,26] For a fixed rate of additive consumption this yields modest changes of the deposition rate in recessed surface features that result in superconformal filling provided the metal ion depletion is not too large[41]. However, more selective, and efficient, void-free filling of high aspect ratio vias can be realized for stronger spatial variation of the deposition rate. This can be realized by positive feedback whereby disruption or burial of the passivating adsorbate occurs at a rate proportional to the local deposition rate. This leads to a much sharper breakdown in suppression that is further amplified at more negative deposition potentials. The dynamics manifest as critical behavior in the form of an S-shaped negative differential resistance (S-NDR) in cyclic voltammetry and highly localized deposition that enables void-free filling of high aspect ratio features.[5-8]

The link between the S-NDR and localized deposition for void-free TSV filling was first demonstrated using suppression provided by coadsorption of ethylenediamine tetrakis(propoxylate-block-ethoxylate) tetrol (TET, Tetronix 701) and chloride ions.[5-7] TSV filling simulations based on disruption, deactivation and/or consumption of the passivating polyether - Cl^- suppressor layer by ongoing metal deposition capture the experimentally observed growth contours.[3,5-8] Electron backscatter diffraction studies reveal the impact of co-adsorbed polymeric-chloride suppressor adlayers on microstructural evolution[42-44] while spectroscopy studies explore incorporation[45,46]. The impact of chloride[45-50] in combination with other adsorbates[5-8,51-67] on Cu deposition is a topic of long-standing interest. There has been substantial study of a range of suppressors, e.g., polyethers, and levelers (e.g., molecules

bearing various nitrogen-groups), that yield both effective S-NDR suppression and localized bottom-up feature filling in acidic Cu electrolytes[51-67] as well as general pattern formation arising from the associated instabilities[68-69].

Herein attention is focused on demonstrating and optimizing the co-adsorption of the TET and chloride ion suppressor precursor chemistry to enable robust "butterfly filling"[2,5-7,15-24] of through glass vias (TGV) as interposers for advanced packaging[70-75]. The filling process initiates with suppressor breakdown and metal deposition concentrated at the center of the TGV.[15-24] Subsequent merging of the deposits on the sidewalls, bridging the vias, thereby dividing the original through hole into two blind vias that are then filled by "bottom-up" void-free progression of the growth front towards the via openings. The ability to fill individual vias can be readily demonstrated by potentiostatic and galvanostatic deposition but uniformity across the work piece has proved challenging due to the critical nature of the passive-active transition, and it is not uncommon to have unfilled, partially filled or voided features.[12,13,15-20]

In an effort to obtain more uniform filling across large TGV arrays, different strategies have been used, among them, different sidewall angle of conical TGV's and pulse electroplating.[19,25,28-31] Different variations have been explored, but, for practical reasons, attention has been focused on pulsed current operation as well as pulse reverse cycles.[19,28-30] In recent simulations of through hole deposition significant differences in filling behavior were noted with variation of the control function.[24] Further still, the nature of the coupling between ohmic losses and electromigration reveals even greater complexity in the control and evolution of S-NDR systems.[26,27] This work aims to further unravel these effects to better understand the nature of through hole filling and to highlight avenues for process optimization by using an asymmetric periodic pulse potential program. The pulse sequence begins with a short potential step to V_{Act} that is negative of the voltametric threshold observed for suppression breakdown

to initiate, restart or fortify active growth in unfilled vias. The (re)activated deposition is not necessarily limited to the recessed regions of the work piece, but the subsequent longer duration step to more positive potential V_{Dep} is such that active deposition becomes localized within the recessed features. Re-passivation of the surrounding field and upper regions of the filling vias under mixed control kinetics serves to even out variations across the via-patterned workpiece. The ability of this approach to enhance filling uniformity is demonstrated as a function of the potentials used for the pulse and deposition steps. The process is repeated as necessary to completely fill the TGV with the progression of feature filling and termination reflected in the associated transients.

EXPERIMENTAL DETAILS

The base electrolyte in this study was composed of 0.88 $mol \cdot L^{-1}$ $CuSO_4$ + 0.5 $mol \cdot L^{-1}$ H_2SO_4 dissolved in 18 MΩ·cm water at room temperature. The polyether TET additive was provided by Aldrich, while the chloride source was NaCl. Additives were dosed from master solutions of refrigerated 2.1 $mmol \cdot L^{-1}$ TET dissolved in 18 MΩ·cm water stock and 100 $mmol \cdot L^{-1}$ NaCl dissolved in 18 MΩ·cm water. Unless stated otherwise, additive concentrations in this study were 100 $\mu mol \cdot L^{-1}$ NaCl and 10 $\mu mol \cdot L^{-1}$ TET. The Pt anode wire was held in a glass tube with a fritted bottom within the cell (i.e., a separated cell) to reduce interactions with the additives during analytical studies. All potentials are reported versus a $Hg/HgSO_4$ (saturated K_2SO_4) reference electrode.

Electrochemical studies were conducted using a Pt rotating disk electrode (RDE) of 0.5 cm diameter that was freshly polished to 1200 SiC grit, rinsed and dried using Ar before each experiment. Through hole filling by electrochemical deposition (ECD) was conducted on glass interposer substrates fabricated by SCHOTT from Borofloat 33 glass using laser-induced deep

etching. The glass substrates, approximately 0.4 mm thick, were patterned with arrays of vias in a nominally 3 × 5 grid of 13 vias (shown in the supplementary material **Figure S1**). The vias are at a pitch of ≈ 340 μm in both in-plane directions (680 μm where vias are omitted within the pattern) with adjacent arrays separated by 680 μm. The vias have a double conical shape, with a narrow waist mid-substrate and increasing diameter toward the free surfaces.

Seeding of the TGV substrates was accomplished by atomic layer deposition (ALD) of either ruthenium or iridium using a TiN nucleation layer for Ru and a TiO_2 nucleation layer for Ir. Depositions were performed on the Forge Nano Theia© ALD reactor employing coordinated pressure control of the deposition area during precursor introduction and purge[76]. All depositions occurred at 250 °C. Precursors were delivered via a showerhead above an aluminum pedestal used to hold the sample carrier. TiN and TiO_2 were deposited with the standard two-step ALD process using $TiCl_4$ and hydrazine[77] or H_2O[78], respectively. Ru and Ir ALD involved three-step ALD processes, referred to as ABC-type ALD. Ru ALD used bis(ethylcyclopentadienyl) Ru(II) ($Ru(EtCp)_2$), ozone (O_3), and hydrogen (H_2), 5 % H_2 in 95 % N_2[79,80] (by volume). Ir ALD used tris(acetylacetonate) Ir(III) ($Ir(acac)_3$), oxygen (O_2) and H_2, 5 % H_2 in 95 % N_2.[81] Growth per cycle was in line with literature for all ALD processes. The quality of the metal films was checked with a 4-point probe using a Keithley 2450 source meter and a Signatone Pro4 manual measurement stand on ALD films deposited on 200 mm Si wafers prior to coating the TGV specimens. Resistivity of a 20 nm Ru film was measured at 22 μΩ·cm and a 10 nm Ir film measured 16 μΩ·cm. The TGV samples were loaded on a 200 mm carrier wafer and held in the chamber 60 s to ensure thermal equilibrium before being exposed to O_3 for 30 s to remove adventitious carbon. Depositions occurred as follows to ensure both faces of the samples were coated with sufficient metal for electrochemical deposition. First, 5 nm of TiN (for Ru) or 1 nm of TiO_2 (for Ir) was deposited. The samples were then removed to

atmosphere, flipped and reintroduced to the chamber. A second TiN or TiO_2 layer of the same thickness was applied. Then, without an air-break, the first metal layer, 20 nm of Ru or 10 nm of Ir, was deposited. Next the samples were removed from the chamber, flipped, then reintroduced to the chamber where the last layer of metal, 20 nm of Ru or 10 of Ir, was deposited. This sequence ensures that the necessary minimum amount of metal ALD film exists on both faces of the samples. It is expected that more ALD film was deposited on the surfaces in the vias. Approximately 20 nm of Ru (or 10 nm of Ir) was deposited on the faces and 40 nm of Ru (or 20 nm of Ir) was deposited in the vias. After deposition, samples were placed in carriers and vacuum sealed**.** Oxidation before use was minimized by storage in a turbo-pumped vacuum better than 1.3×10^{-6} Pa (1×10^{-8} Torr).

For Cu filling, fragments of the patterned specimens approximately 0.5 cm × 1.5 cm were mounted into a slot in the side of the RDE rotator spindle along one shorter edge so that the specimen rotates around it like a helicopter blade, but without inclination. The geometry enabled nominally laminar flow across the specimen surfaces during deposition. The projected area of the patterned substrates exposed to the electrolyte was approximately 1 cm^2 (i.e., each side 0.5 cm^2). Measured values were used to normalize the measured currents to current densities.

Despite vacuum storage, additional surface preparation of the ALD-seeded TGV specimens was typically necessary prior to the Cu filling process.[82,83] The mounted specimens were first wetted with ethanol and then immersed in a cell containing 0.5 $mol \cdot L^{-1}$ H_2SO_4 and held at -0.4 V for a minimum of 1 min to reduce air-formed oxide; more negative potentials yielded more rapid reduction of oxide but risked the formation and trapping of hydrogen bubbles within the vias. The substrates were then quickly transferred, while still wet, to a cell containing 0.88 $mol \cdot L^{-1}$ $CuSO_4$ + 0.5 $mol \cdot L^{-1}$ H_2SO_4 for 10 min of deposition at -0.48 V to form fresh,

nominally identical Cu-seeded surfaces on all substrates. The ALD (Ru or Ir)/ECD Cu-seeded specimens were then transferred, while still wet, to the additive-containing electrolyte for the filling experiments.

To image the Cu-filled TGVs by optical microscopy, the post-deposition specimens were encapsulated between glass coverslips using epoxy and then polished in cross section on diamond lapping papers down to 1 μm grit. The cross-sections were oriented to permit simultaneous viewing of rows of vias in multiple arrays parallel to the longer edge of the specimen, which correspond to a monotonic increase in radial velocity, and thereby fluid flow across the vias during Cu deposition. For each specimen vias were examined within a minimum of two rows between the trailing edge and midline of the substrate by successive polishing and imaging steps.

RESULTS

Electrochemical behavior of the Cl^-–TET additive system

Cyclic voltammetry probing Cu deposition in the additive-free electrolyte and following the addition of different combinations of Cl^- and TET additives is shown in **Figure 1**. The measured currents were converted to current densities assuming uniform deposition across the surface of the RDE, which in case of non-uniform deposition might overestimate the active area, and thus underestimate the active current density, at potentials immediately negative of suppression breakdown.

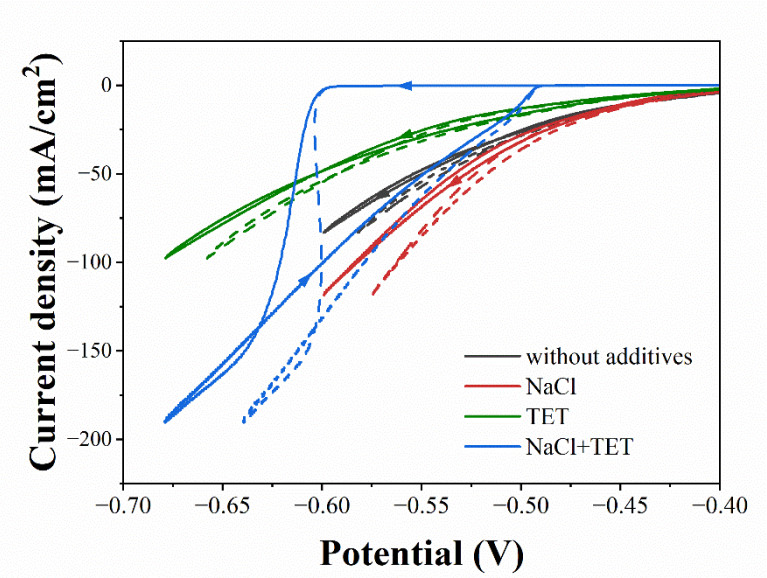

Figure 1. Cyclic voltammograms of Cu electrodeposition obtained at 2 mV·s^{-1} on a 0.5 cm diameter RDE rotating at 100 rpm (200π rad·min^{-1}) in 0.88 mol·L^{-1} $CuSO_4$ + 0.5 mol·L^{-1} H_2SO_4 with the indicated combinations of 100 μmol·L^{-1} Cl^- and 10 μmol·L^{-1} TET additives. All cycles were initiated at the open-circuit potential of –0.36 V and collected using 80 % current × resistance (iR) software compensation of the measured ohmic cell resistance of R = 5.3 Ω (solid curve). Voltammograms after full correction for system resistance are also shown (dashed curve).

The addition of Cl^- to the bare electrolyte provides modest increase of the deposition rate relative to the additive-free case, consistent with the known ability of adsorbed Cl^- to accelerate Cu^{2+} reduction[47]. The addition of TET alone yields modest polarization that might be partly aided by trace Cl^- contamination associated with the $CuSO_4$ source material. In contrast, strong suppression on the negative-going scan is obtained in the presence, and co-adsorption, of both (more substantial) Cl^- and TET additions. The very low current density across the negative-going scan in this case indicates a strongly passivated surface state is maintained until

suppression breakdown occurs near -0.6 V. The critical nature of the suppression breakdown is reflected in the negative differential resistance associated with the S-shape in the fully iR compensated voltammetry. Comparison to voltammetry for electrolyte with only Cl^- added suggests that a fully activated (i.e., unsuppressed) surface is rapidly obtained upon suppression breakdown and that this state is retained during the remainder of the negative-going scan. The activated state is maintained on the positive-going return scan until suppression is reasserted at approximately -0.49 V, substantially positive of where suppression breakdown occurred. The resulting hysteresis marks a potential range within which different regions of the electrode surface can exhibit very different deposition rates reflecting co-existence of the active and passive states. Given the previously detailed dependence of suppression breakdown potential on additive concentrations[64,65], preferential breakdown of the suppressor adsorbate complex and localized deposition may be anticipated within recessed features due to transport-related delays in the additive adsorption and gradients of the additive concentrations that combine to enable superconformal filling of TGVs at potentials within the range -0.6 V and -0.49 V.

TGV Filling at Fixed Potential

An example of via filling in the additive-containing electrolyte is shown in **Figure 2**. The potential of -0.56 V for the deposition falls toward the middle of the hysteretic region obtained with the RDE in **Figure 1**. The coexistence of regions of passive and active deposition is readily apparent, with active deposition generally localized within the recessed vias due to the transport-constrained fluxes of the suppressing additives, although some limited active deposition is still observed on the field. A less negative deposition potential and/or increased additive transport through higher rotation rate or additive concentrations will enhance localization toward the bottoms of the vias. However, for the given conditions only one via in

this array has fully filled while the other vias exhibit negligible deposition or something in between. The critical nature of suppression breakdown in this electrolyte-additive system makes the nucleation of suppressor breakdown and maintenance of active deposition highly susceptible to local variations of geometry and fluid flow. Consequently, potentiostatic deposition is not well suited for via filling with the given hydrodynamic conditions and electrolyte.

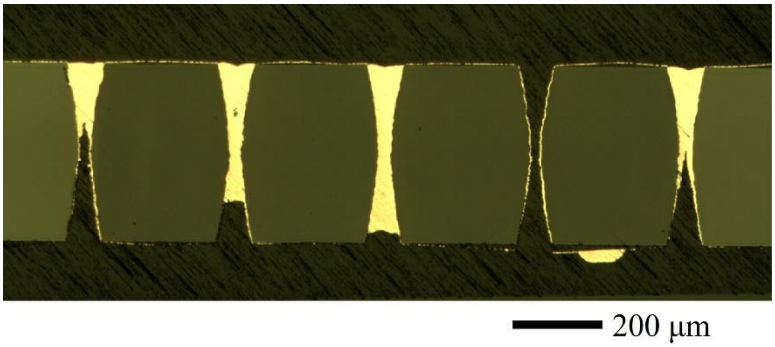

Figure 2: Optical metallographic cross section of Cu filling of TGVs in the fully constituted electrolyte after 30 C deposited at –0.56 V (≈ 2 h and 25 min) while rotating at 25 rpm.

Exploring Asymmetric Pulsed Potential Deposition Parameters for TGV Filling

As an alternative to potentiostatic filling, a periodic pulse process entailing a short step of the applied potential to a value negative of the potential of suppression breakdown followed by a substantially longer period of deposition at a potential in the hysteretic potential range was examined. The perturbation waveform is characterized in the schematic shown in **Figure 3**, with the potential V_{Act} applied as a short (1 s) activation pulse followed by stepping of the potential to V_{Dep} for an extended period of 10 min. An empirical parameterization of the resulting current transients is outlined in the same figure. The average current density J_{Act}

during the pulses is a measure of the passive area that is activated by breakdown of the suppression layer, in addition to increase of the current density on passive and active areas at the more negative potential. The maximum and minimum current densities during the deposition step, J_{Max} and J_{Min}, respectively, serve as measures of the changing active area during the deposition step; i.e., the difference J_{Max} - J_{Min} reflects the loss of area activated by the pulse to V_{Act} through re-passivation during the deposition step. The time t_{Dec} captures the current decay to a steady state that reflects the timescale for re-passivation of some, or all, of the area activated during the pulse. Because suppression breakdown on the RDE occurred at –0.60 V in the fully constituted electrolyte (**Figure 1**), potentials negative of -0.60 V are logical targets for the activation pulse while potentials positive of -0.60 V are logical values for localization of sustained deposition.

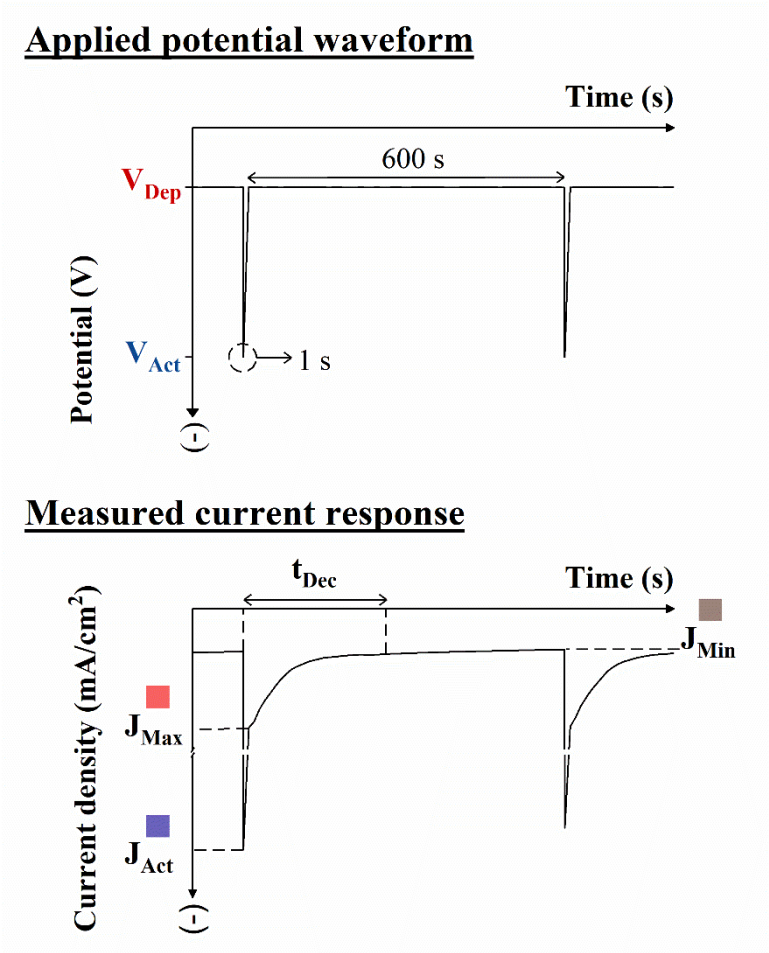

Figure 3: Schematic of one periodic pulsed deposition cycle that involves a 1 s pulse to the activation potential V_{Act} followed by a 600 s hold at the deposition potential V_{Dep}. The resulting current transients are characterized by the current density J_{Act} during the V_{Act} pulses, the maximum J_{Max} and minimum J_{Min} current densities during the V_{Dep} deposition step and the time t_{Dec} required to stabilize deposition following the pulse; a value of 10 min for the last is used to indicate the current did not stabilize during the deposition step.

In this exploration, following immersion in the fully comprised electrolyte, the freshly Cu-seeded TGV substrates were held for 5 min at -0.40 V to fully passivate the surface and then the pulsed process was initiated to sequentially, without interruption, examine the impact of

different V_{Dep} and V_{Act} potentials on the Cu deposition process. The current transient for variation of the former is shown with the extracted parameters in **Figure 4**. The study progressed with a monotonic shift of V_{Dep} to more negative potentials to reduce cumulative deposition from the preceding cycles, given the lower deposition rates and more localized deposition anticipated at less negative potentials. The potentials for the deposition step were restricted to values positive of -0.54 V, less negative values of the hysteretic range, to promote re-passivation of the field. Anticipating gradients of additive concentrations within the tall vias, deposition potentials as positive as -0.44 V were examined despite their being positive of the -0.49 V value at which re-passivation occurred on the RDE. The pulse potential of -0.68 V is 80 mV negative of suppression breakdown to ensure significant activation across the workpiece.

The exploration of deposition potentials in **Figure 4a** yields a smooth and modest increase in the magnitude of both J_{Max} and J_{Min} (see **Figure 4c**) as V_{Dep} is advanced from -0.44 V to –0.52 V. At -0.54 V the current densities increase suddenly and more substantially and also become less repeatable, especially J_{Max}. The difference J_{Max} - J_{Min} changes monotonically (–33, –65, –80, –110 and –750) $\mu A \cdot cm^{-2}$ as the potential advances from -0.46 V to -0.54 V. Like the individual quantities, it manifests a gradual increase to -0.52 V and substantial change at -0.54 V. The transients in **Figure 4a** and extracted decay time t_{Dec} in **Figure 4d** show that the decrease to steady state J_{Min} following each pulse takes longer as V_{Dep} shifts more negative; it is a small fraction of the hold time at -0.46 V but reaches/exceeds the 10 min window for deposition at both -0.52 V and -0.54 V.[†] Importantly, the transition to steady-state behavior does not preclude continued active deposition over some area of the specimen. However, the case of

[†] The results at -0.44 V are not considered here. The inverted transients, with current density increasing after each pulse, indicate another effect underlies the behavior. The very low currents also make the condition of less practical importance.

continuing decay over the 10 min of deposition at both -0.52 V and -0.54 V is taken as an unambiguous sign that at least some of the area freshly activated at V_{Act} remains active during this period.

From a practical perspective, rapid re-passivation means that deposition on freshly activated surface area is not sustained, which can hinder bottom-up filling. Conversely, re-passivation that is too slow may allow substantial deposition in undesirable areas, such as sidewalls near the openings of filling features or on the field. Indeed, the much higher current density at -0.54 V indicates just such a change in the activated geometry; post-deposition inspection of this and other specimens indicates that the increased current density corresponds to undesirable deposition at locations on the field of the substrate.

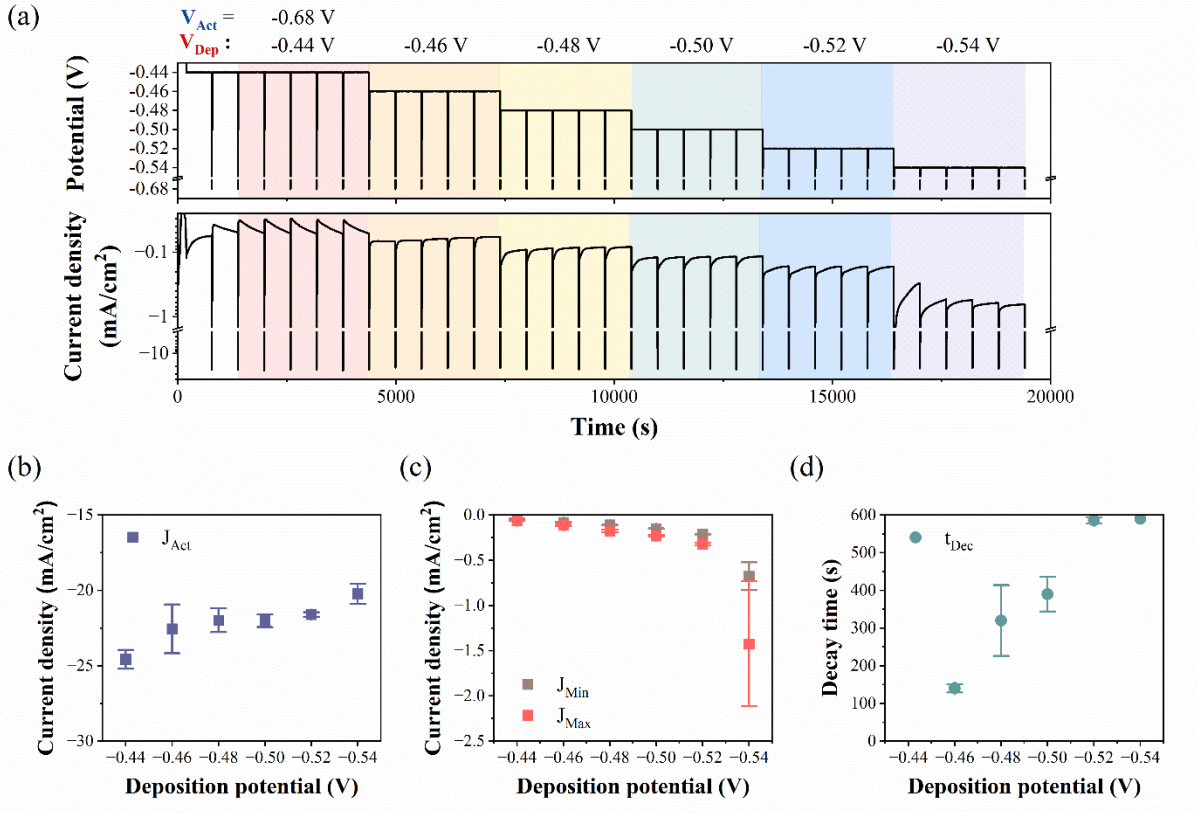

Figure 4: a) Applied potential and resulting current density during deposition on an interposer specimen patterned with 208 through vias in the fully constituted electrolyte while the

specimen was rotating at 100 rpm. The surface of the Ru/Cu seeded substrate was first passivated by deposition for 5 min at -0.40 V. The potential was then cycled through 1 s at -0.68 V and 10 min at -0.44 V and then, after six or five cycles, V_{Dep} advanced to -0.46 V, etc., as indicated. b) Extracted values of current density J_{Act}, c) maximum and minimum current densities J_{Max} and J_{Min}, respectively, and d) decay time t_{Dec} associated with stabilization are averages of the five transients for each deposition potential, or the final five transients in the case of -0.44 V. The error bars indicate the standard deviation of the values obtained. Given the substrate area of ≈ 1 cm^2, ohmic losses due to the uncompensated ≈ 5 **Ω** system resistance exceed 50 mV during the V_{Act} pulses but range from less than 1 mV to approximately 5 mV during the V_{Dep} steps.

An analogous experiment explored different V_{Act} potentials with current densities and time scale extracted from the transients shown with the results in **Figure 5**. Based on the voltammetry, the nominal V_{Act} potentials for activation should achieve a fully activated surface. However, the actual electrode potential is impacted by uncompensated ohmic losses in the electrolyte due to the high current density of activated regions at potentials negative of –0.60 V (see **Figure 1**). Activation potentials V_{Act} over the range –0.62 V to –0.71 V were examined to accentuate and reveal the consequence of such effects. In these experiments the V_{Dep} potential was set to -0.52 V as the least negative value for which active deposition was definitively maintained throughout the pulse sequence and the most negative potential for which repeatable transients were observed in the preceding experiment (see **Figure 4a** and **4c**).

The average current density during the pulses J_{Act} increases with overpotential as summarized in **Figure 5b**. The V_{Act} change from –0.62 V to -0.65 V induces the largest

fractional (but not absolute) increase in peak current. The linear potential dependence negative of -0.65 V largely reflects the impact of ohmic losses along with the kinetics of the de-passivation at potentials near the critical value for suppression breakdown. Despite the greater than 25× increase of current density during the V_{Act} pulses, their short 1 s duration results in little Cu deposition. Also, beyond the first hour of the pulse program, there is little impact of the activation potential step on the current density during the subsequent V_{Dep} deposition steps[‡]. The current densities J_{Max} and J_{Min} in **Figure 5**, being all obtained at the same deposition potential, can be treated as measures of the active deposition area. Both values increase only modestly for more negative pulse potentials.

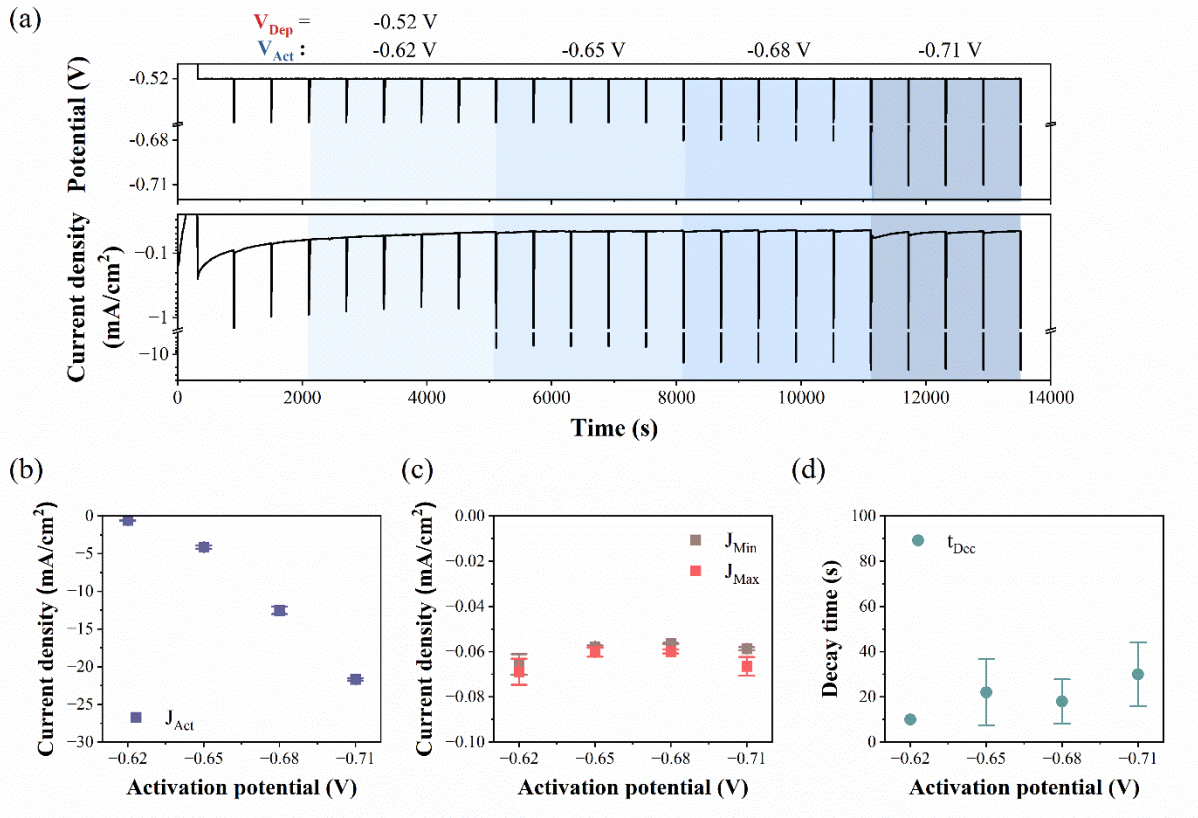

Figure 5: a) Applied potential and measured current during deposition on an interposer

‡ The gradual decay of deposition current over the first hour is evidently related to the use of freshly constituted electrolyte.

specimen patterned with 208 through vias in the fully constituted electrolyte while the specimen was rotating at 100 rpm. The surface of the Ru/Cu seeded substrate was first passivated by 5 min deposition at -0.40 V. The potential was then cycled through 1 s at -0.62 V (then -0.65 V, etc., as indicated) and 10 min at -0.52 V; 7 cycles were used at the first potential, and 5 cycles were used for the remaining potentials. b) The pulse current density J_{Act}, c) the maximum and minimum current densities J_{Max} and J_{Min}, respectively, and d) the decay time t_{Dec} associated with stabilization are averages of the five results at each value of the pulse potential (the final five at -0.62 V). The error bars indicate the standard deviation of the values obtained. For substrate area of ≈ 1 cm^2, ohmic losses due to the uncompensated ≈ 5 **Ω** system resistance range from less than 5 mV to more than 50 mV during the activation pulses but are less than 1 mV during the extended deposition steps.

For the sake of completeness, it is noted that the exploration of activation potential V_{Act} in **Figure 5** and the exploration of deposition potentials V_{Dep} in **Figure 4** share a common pairing of V_{Act} at -0.68 V and V_{Dep} at -0.52 V. More effective activation during the pulses is evident in the study of V_{Dep} (compare **Figure 4b** and **Figure 5b**) for which there are more preceding cycles and associated deposition (compare **Figure 4a** and **Figure 5a**) due to the different potential histories. The freshly constituted electrolyte used to obtain the results in **Figure 5** was subsequently used to obtain the results in **Figure 4**. Should the difference reflect some change in the electrolyte despite the use of a separated cell for the anode, then one might be inclined to favor the latter (and later) data as the via filling experiments involve more cycles than the two exploratory experiments combined (vide infra).

Asymmetric Pulsed Potential Filling of TGV

Given the highly variable TGV filling observed for deposition at fixed potential (**Figure 2**), specimens were examined after deposition involving different numbers of pulse cycles to follow the via filling evolution. TGV filling using the activation and deposition potential combination of 1 s at -0.68 V and 10 min at -0.52 V, respectively, that exhibited sustained and repeatable activation in the exploratory studies is shown in **Figure 6**. The three specimens, with filling halted after 36, 72, and 96 cycles, correspond to total deposition times of 6 h, 12 h, and 16 h, respectively. Cross-sectioned via arrays presented in **Figure 6a** capture the evolution of feature filling. After 36 cycles substantial variation, like that observed with fixed potential, is evident, with some of the conical vias only just starting to fill, others filled only in one half and others completely filled. Deposition at this earliest sampling time appears stochastic in its distribution, presumably the result of differences in substrate or feature geometry or electrolyte flow or composition; the apparent bias of filling toward one surface likely reflects a difference in flow along the upper and lower surfaces of the rotating "helicopter-blade" specimen arising from asymmetry of geometry or mounting on the RDE mandrel. The uniformity of filling improves with increased cycles, with further deposition and substantial improvement in uniformity evident by 72 cycles and via filling complete across the sampled array by 96 cycles. Significantly, unlike the fixed potential deposition, there are no large deposits on the field, only a rough surface deposit due to repeated activation and re-passivation of the free surface. The consistency of via filling across the substrates is captured in images of eight groups of vias from each specimen in the supplement (**Figure S2**).

The current transient for the 16 h deposition is shown in **Figure 6b**. Given the large number of vias across the area of the specimen one might anticipate a smooth and monotonic change of the deposition current during the cyclic process through averaging of the passivation and

activation of individual vias. However, comparatively slow and (fractionally) substantial variation of current over the course of multiple 10 min deposition steps is evident. Despite this variation, the cross-sectioned specimens demonstrate that continued deposition improves the uniformity of filling across the substrate. Notably, deposition in later filling vias is accomplished without overfill of vias filled earlier; re-passivation as Cu fill approaches the field is very effective for these conditions. Likewise, deposition in the fully filled vias is hardly reactivated by the pulsing, or, more importantly, if it is, it does not remain activated for long. It is also necessarily true that, in vias that remain unfilled after early cycles, reactivation occurs during subsequent pulse cycles, enabling completion of via filling. Finally, the absence of large deposits on the field after 16 h indicates that the pulse potential process is effective in interrupting runaway growth instabilities that often develop during potentiostatic operation. That said, the increased roughness on the free surface reflects short periods of randomly distributed active deposition associated with the gradual passivation and modest current decay during the deposition steps in each cycle, just visible in **Figure 6b** following the step back to V_{Dep} from the activation pulses. Any impact of change in the active growth area as filling progresses from the midline of the vias to the field is evidently obscured by the randomized filling manifest at earlier times and the distributed (re)activation favored by the pulsed process. The increasing roughness on the field does, however, appear to manifest in a monotonic increase of the elevated J_{Act} current density during the pulses beyond the first cycle.

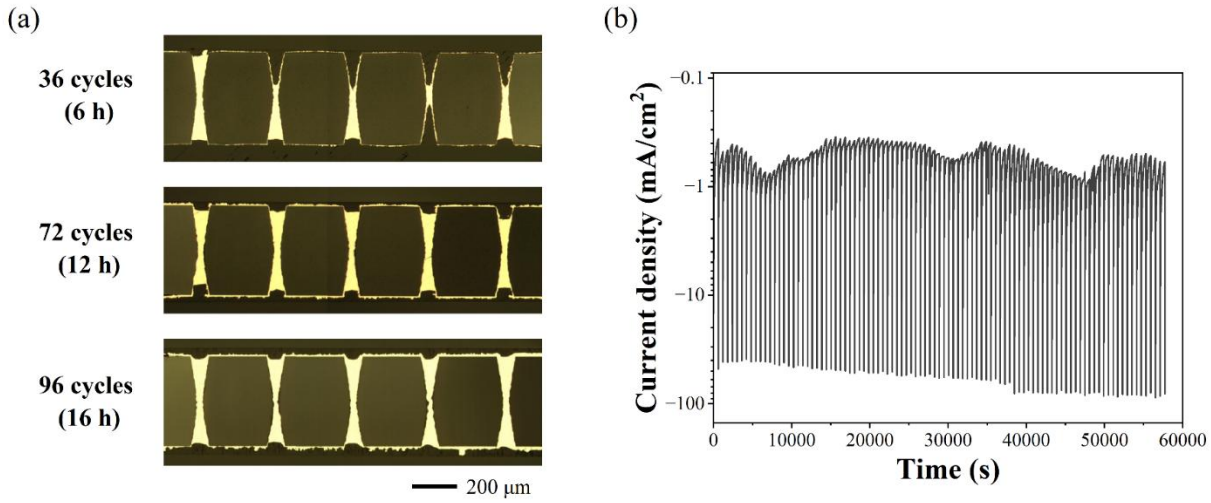

Figure 6: TGV filling in the fully constituted electrolyte by cycling the potential between (V_{Act}) -0.68 V for 1 s and (V_{Dep}) –0.52 V for 10 min while the specimens were rotating at 100 rpm. a) Cross-sectioned vias imaged optically after filling for the indicated number of cycles. b) The current density transient for the specimen filled over 96 cycles. For a substrate area of ≈ 1 cm^2, ohmic losses due to the uncompensated ≈ 5 Ω system resistance exceed 100 mV during the pulses but are less than 5 mV during the deposition steps.

Filling after 96 cycles was also examined for different V_{Dep} potentials with V_{Act} fixed at -0.68 V as used in the exploratory experiments (**Figure 4**). Cross-sectioned vias are shown in **Figure 7a**. For V_{Dep} of –0.44 V the entire surface remains fully passive, with no evidence of active deposition in comparison to the as-fabricated ALD/ECD seed layers shown in the same figure. With more negative V_{Dep} the bottom-up localized deposition growth front extends farther from the via middle toward the via openings. The trend is analogous to the increase of fill height in TSV with overpotential seen in S-NDR electrolytes for not only Cu but also Co[36] and Ni[40].

A single snapshot of the filling process at 16 h provides neither complete nor unambiguous information regarding the detailed evolution of filling. For example, the deposit could reflect active growth from small active regions at the via centers extending progressively over different periods of time at the different deposition potentials, or growth might occur by more extended sidewall activation at more negative potentials followed by some degree of lateral growth. That said, with one of the vias at 36 cycles in the sequential filling results (**Figure 6**) exhibiting bridging only at the narrow waist of one conical via, the former appears to be the case at -0.52 V, and it is not unreasonable to surmise that growth at the less negative potentials evolves similarly. The current transients at V_{Dep} for cycles near the start, middle and end of the deposition processes are shown in **Figure 7b**. Although the current is elevated immediately after the pulse for deposition at both -0.44 V and -0.46 V, it decays rapidly; indeed, the initial rate of decay might be obscured by the 10 s sampling interval used for data acquisition during the 10 min deposition steps. In contrast, the elevated current density following the pulse at the more negative values of V_{Dep} decays over a longer period, particularly in the earlier cycle.

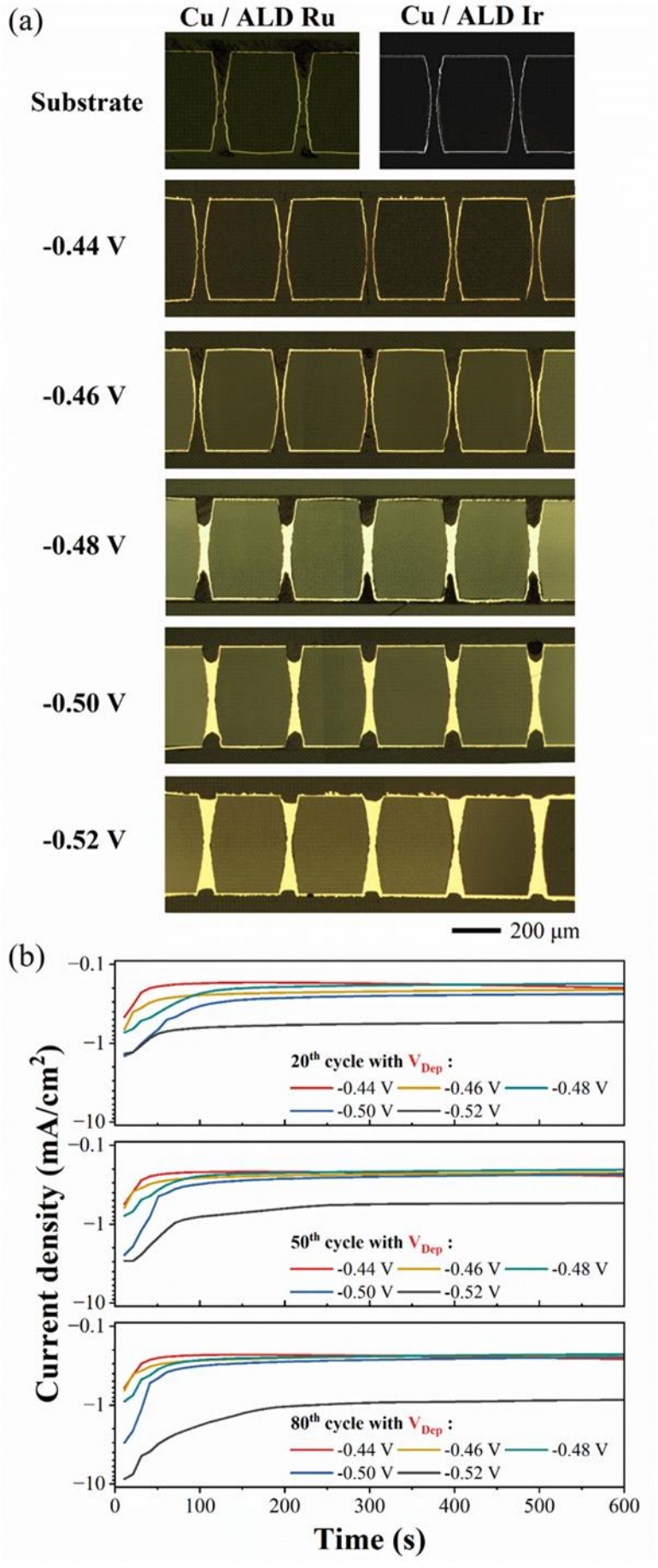
(a)
Cu / ALD Ru
Cu / ALD Ir
Substrate
-0.44 V
-0.46 V
-0.48 V
-0.50 V
-0.52 V
200 μm
(b)
Current density (mA/cm²)
20th cycle with V_Dep :
50th cycle with V_Dep :
80th cycle with V_Dep :
-0.44 V
-0.46 V
-0.48 V
-0.50 V
-0.52 V
−0.1
−1
−10
0
100
200
300
400
500
600
Time (s)

Figure 7: TGV filling in the fully constituted electrolyte after cycling the potential 96 times (16 h) from V_{Act} –0.68 V for 1 s to V_{Dep} ranging from -0.44 V to -0.52 V for 10 min while the specimens were rotating at 100 rpm. a) TGV with ALD (Ru or Ir)/ECD (Cu) seed layers alone and after filling at the specified V_{Dep} cross-sectioned and imaged optically. b) The current density transients at the specified V_{Dep} during the 20^{th}, 50^{th} and 80^{th} deposition cycles. The ohmic losses do not exceed 5 mV during the deposition steps based on a substrate area of ≈ 1 cm^2 and uncompensated ≈ 5 Ω system impedance.

Comparison of the responses at different cycles suggests that the current transient decays more rapidly in later cycles for deposition at -0.48 V and -0.50 V while it remains elevated for deposition at -0.52 V. The transients for V_{Dep} in the range -0.44 V to -0.50 V asymptote toward a similar value while the current at -0.52 V remains elevated. Several important conclusions can be drawn through comparison with the cross-sectioned specimens. Firstly, as minimal deposition is evident after 96 cycles with V_{Dep} of -0.44 V and -0.46 V, their current transients can be taken as background signals for assaying the active deposition associated with Cu filling evident in specimens filled using V_{Dep} of -0.48 V, -0.50 V and -0.52 V. Further, the transients for -0.46 V through -0.50 V converge after a few hundred seconds, especially in later cycles. Taken together, these observations indicate that the bulk of the Cu filling occurs during the first 100 s as re-passivation takes hold across most of the work piece. This offers the prospect of shortening the dwell time at V_{Dep} to improve the overall via filling efficiency. With V_{Dep} increased to -0.52 V, however, significant deposition is evident on the field, and this is associated with the elevated current density sustained throughout each and all cycles in the process.

A more comprehensive view of the evolution of the current transients with cycling is

provided for each V_{Dep} in **Figure 8**. While the current density transient for V_{Dep} of -0.44 V in **Figure 8a** drifts initially, it settles after ≈ 30 cycles. Similarly, for V_{Dep} of -0.46 V the transients in **Figure 8b** are essentially identical between 20 to 90 cycles. In comparison, the corresponding TGV in **Figure 7a** reveal no evidence of significant deposition for V_{Dep} of -0.44 V, and, for -0.46 V, only the earliest stage of growth at the middle of the vias, with minimal net shape or area change, is evident. Both results are also consistent with the similarity of the corresponding current transients in **Figure 7b**.

In contrast, for V_{Dep} in the range -0.48 V to -0.52 V that yield progressively increased TGV filling in **Figure 7a**, the corresponding transients in **Figure 8** exhibit progressively larger changes. For -0.48 V an increased current density is obtained for the first ≈ 75 s of the earlier cycles (**Figure 8c**) in addition to a small, but systematic, increase in the steady-state current with increasing number of cycles. The changes accompany splitting of the through-hole into two blind vias and development of a concave active growth front as seen in **Figure 7a**. For V_{Dep} of -0.50 V a comparatively higher initial deposition current decays over ≈ 150 s during the earliest (10^{th}) cycle recorded in **Figure 8d**. The post-pulse current density increases with further cycling, achieving a more defined peak shape by the 30^{th} cycle that is sustained thereafter. The current associated with this post-pulse transient decays more rapidly with further cycling, yielding a more compressed transient to the steady-state current density of -0.23 mA/cm^2 that is stable by the 60^{th} cycle. As noted with **Figure 7b**, this steady state current density is similar to that observed at the more positive V_{Dep}.

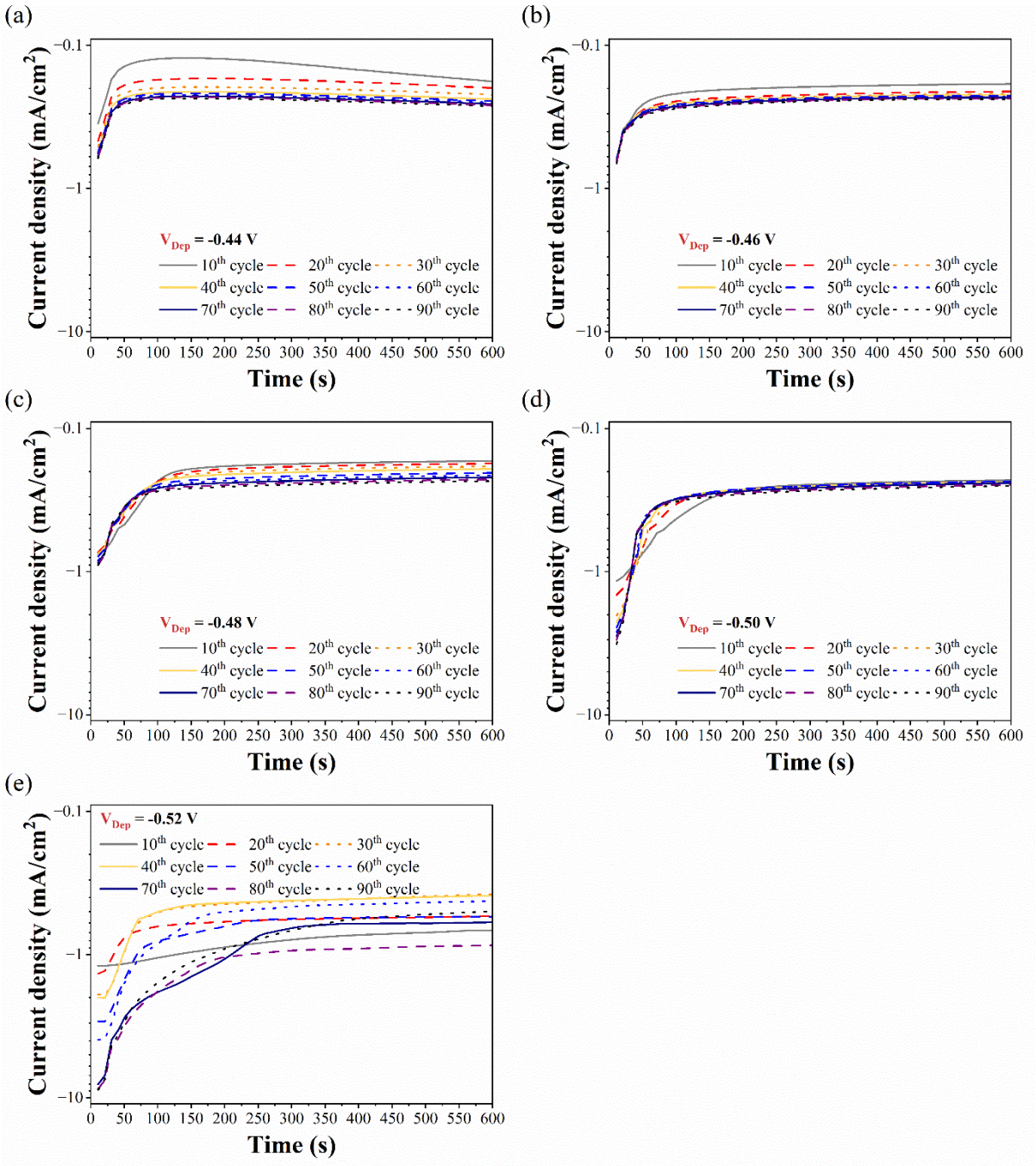

Figure 8: Current density transients at V_{Dep} for the 10th, 20th, 30th, etc., cycles during filling of the specimens shown in **Figure 7a** at the specified deposition potentials. The transients capture significant activation and re-passivation following the -0.68 V activation pulses.

Taken together, the feature filling and transients for V_{Dep} of -0.44 V to -0.50 V suggest that a significant amount of the Cu deposition is associated with the first 50 s or 100 s of the 600 s transient period. Indeed, as the system was open to atmosphere, it is likely that a significant portion of the similar, low steady-state currents at later times is associated with O_2 reduction, the electrolyte not being deaerated; the current efficiency was not evaluated. In contrast to the lower potentials, for V_{Dep} of -0.52 V elevated current density is maintained throughout the full 600 s of the 10^{th} cycle, and the post-pulse peak that develops is accompanied by a decaying transient that both increases in size and extends to longer times with further cycling. Comparison of the feature filling in **Figure 7a** and transients in **Figure 8** suggests that this elevated current is associated with the excess build-up on the field.

The effect of the activation potential V_{Act} on TGV filling was also examined after 96 cycles using V_{Dep} of -0.52 V from the exploratory study in **Figure 5**; the most negative activation potential of -0.71 V was not considered given the roughening already evident on the field at -0.68 V. A cross-sectioned group of vias is shown for each potential in **Figure 9a**. All three potentials exhibit localized deposition indicative of some period of surface activation. Further, and in analogy to the trend observed with variation of V_{Dep}, the filled region extends farther from the via middle toward the via openings at more negative V_{Act}. Once again, a single specimen does not by itself indicate the exact origin or evolution of the filling. That said, however, the long-term evolution of the current transients during the 10 min steps at V_{Dep} shown in **Figure 9b** can be meaningfully compared as all are at the same potential. For V_{Act} of -0.62 V the current density even during the activation step itself only reaches -1 $mA \cdot cm^2$ and the subsequent current density at V_{Dep} is essentially constant even immediately after the pulses

beyond the first two or three cycles[§]. The net result of the limited activation provided by excursion to -0.62 V is deposition evident only on the sidewalls of the via middle. In contrast, activation at -0.65 V yields a current peak near -30 mA·cm^2 and current density that varies substantially during the subsequent deposition steps at V_{Dep}. The post-activation currents in the earliest cycles are quite elevated and decay over the full 10 min cycle, but both the peak amplitude and duration of these deposition transients decrease essentially to zero after ≈ 11 cycles. Pulsing at V_{Act} of -0.68 V yields further elevation of the current during activation followed by decay of deposition at V_{Dep} that extends throughout the deposition step throughout the filling experiment (with substantial long-term oscillations already noted with **Figure 6**).

The charge density associated with the transient shown in **Figure 9b** for V_{Act} of -0.62 V corresponds to a deposition charge density of -1.2 C·cm^{-2} using the steady state value as a baseline, with nearly half in the first cycle and the remainder reflecting gradual decay of the baseline. Based on an individual via volume ≈ 1.0 × 10^6 μm^3, average substrate area 3.8 × 10^{-3} cm^2 per via (both surfaces and 20 arrays on the 0.5 cm × 1 cm substrates), 7.1 cm^3·mol^{-1} for fully dense Cu, n = 2 for Cu^{2+} and Faraday's constant 96485 C·mol^{-1}, this charge density is approximately 15 % of the -7.5 C·cm^{-2} value calculated for complete filling, which value is not inconsistent with the deposition visible in **Figure 9a**. The charge density associated with the transient shown for V_{Act} of -0.65 V, relative to its steady-state baseline, is -2.3 C·cm^{-2} or approximately 30 % of the charge density for complete filling and consistent with the filling observed. In contrast, the charge density associated with each of the cycles for V_{Act} of -0.68 V, obtained using the baseline value for V_{Act} of -0.65 V, averages 3.5 % of the value for via filling;

[§] The current decays over the course of the full filling experiment to a lower steady-state value that is more consistent with that at -0.65 V. The experiment was conducted in freshly constituted electrolyte, and the decay is analogous to that noted in **Figure 5**.

deposition in the 96 cycles of the full process is thus several times that expected for full filling of just the vias.

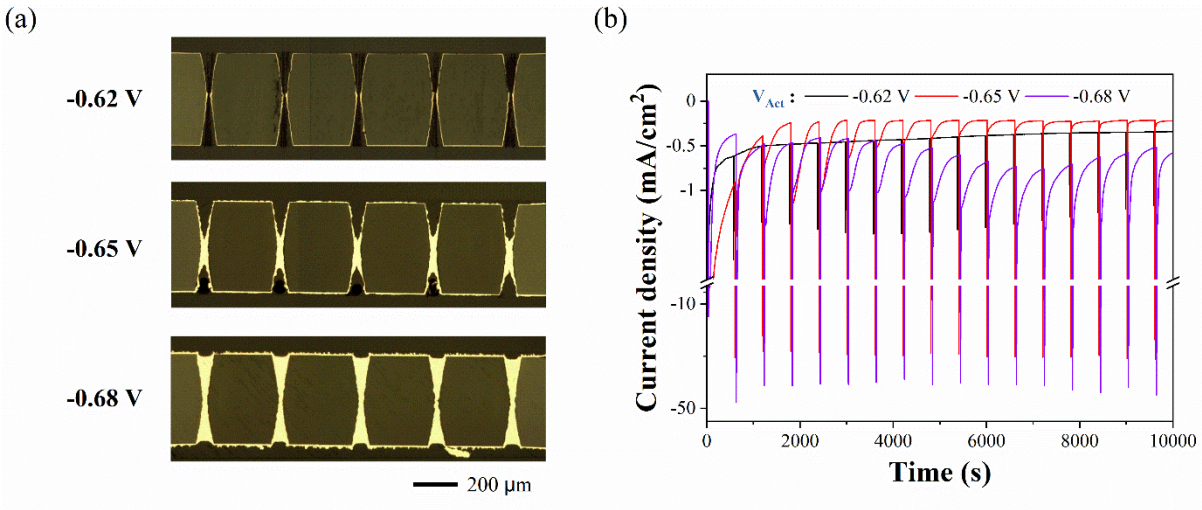

Figure 9. TGV filling in the fully constituted electrolyte after cycling the potential 96 times (16 h) over the indicated activation potential V_{Act} in the range -0.62 V to -0.68 V for 1 s, as specified, followed by 10 min at -0.52 V while the specimens were rotating at 100 rpm. a) Optical images of the cross-sectioned vias after filling using the specified V_{Act}. b) The current density transients during the first several hours of deposition; the transients have been offset slightly in time so the pulses at the different potentials can be differentiated. Ohmic losses vary substantially during the pulses at V_{Act}, but they do not exceed 5 mV during the 10 min deposition steps at V_{Dep} based on a substrate area of ≈ 1 cm^2 and uncompensated ≈ 5 Ω system resistance.

DISCUSSION

For robust void-free filling of high aspect ratio TGV, deposition must initiate within the central region of the via over an area sufficiently localized that variation of the metal ion

concentration does not yield filling with a keyhole void. After bridging of the active deposits on the opposing sidewalls, deposition needs to remain localized to the bottoms of the recessed surfaces of the two newly established blind vias to yield progressive filling toward the via openings. Throughout, deposition on the via sidewalls nearer the openings and outer surfaces of the substrate must remain suppressed. For a given electrolyte and potential control, maintaining such suppression over the longer distance from the openings of larger and deeper features will require reduced overpotential even as propagation of active deposition toward the feature openings, where additive concentrations are higher, may require subsequently increased overpotential.

From a practical perspective, variations of concentration or flow across the substantially larger dimensions of a substrate can localize activation across the substrate area in a manner analogous to the localization that occurs within a particular via. Active areas in vias located within regions that experience reduced suppressor concentrations may be so large that voiding occurs; vias in regions with comparatively higher additive concentrations may passivate entirely. In analogy to the process variation required for controlled filling within the vias, more positive deposition potentials may be needed to restrict the active area in less suppressed areas while more negative potentials may (subsequently) be required to activate and promote filling in more suppressed areas. Reflecting the hysteretic nature of deposition in S-NDR additive-containing electrolytes, activation of passive surfaces may require a quite negative potential, e.g., for this electrolyte, negative of the -0.6 V potential of suppression breakdown, even as substantially more positive values in the hysteretic window are needed to initially localize deposition in deeper features. In the present electrolyte, via filling to the field will, as with the RDE, require a potential negative of -0.49 V.

This study has utilized a periodic asymmetric two-potential step process that intermittently

provides surface activation in all vias followed by deposition driven more modestly at potentials within the slow scan rate (< 10 mV·s) hysteretic voltametric window. The process achieves faster deposition in less-filled vias and slower deposition in more-filled vias to enable complete and void-free filling of all the vias, presumably by taking advantage of gradients of suppressor additive-concentration within the recessed features.[**] The asymmetric pulse potential process overcomes via-to-via variation of filling that otherwise arise during deposition in the critical system where even small differences in via geometry and macro- and micro-scale gradients of potential, electrolyte flow and concentrations can trigger bifurcation in undesired locations.

With application of the asymmetric pulse scheme, electrolyte containing the Cl^--TET additives previously used for bottom-up superconformal filling of TSV also yields more robust filling of the through hole vias in glass interposers. The experimental evolution, although not quantitatively compared, is consistent with prior simulations for cylindrical vias[24,27] based on the S-NDR mechanism. Filling is characterized by initial localization of deposition toward the feature center, followed by broader expansion of deposition at more negative potentials. In the case of through-holes this includes sidewall fusion or bridging that forms two blind vias followed by bottom-up growth toward the via openings. The asymmetric pulse potential TGV filling process also exhibits a potential-dependent depth of the passive-active transition that is analogous to that observed and predicted in filling of TSV.

Despite the obvious contrast between initial deposition in TGV through holes and blind TSV, the asymmetric pulsed deposition approach leads to the same evolution, namely, growth

[**] It thus differs fundamentally from pulsed deposition processes wherein the longer hold step involves minimal deposition and thereby serves to allow relaxation of gradients of (metal ion) concentration developed through deposition during the shorter pulse.

propagation proceeding from locations that are less suppressed to locations that are more suppressed. Given the anticipated/predicted utility of the S-NDR mechanism for filling the TGV geometry, the potentials for both the short (1 s) activation pulse at V_{Act} and the long (10 min) deposition step at V_{Dep} were derived from cyclic voltammetry measurement of the suppression breakdown and the hysteretic window. The TGV filling studies support these choices.

That said, the filling times obtained here are long. For comparison, filling times from 1 h to 12 h have been described for electrolytes using different additives to obtain localized butterfly filling of through vias of similar size (see Ref. 21 and introduction). The results obtained here reflect the range of deposition potentials compatible with filling in this S-NDR electrolyte, a a subset of more positive potentials defined by the hysteretic range of the CV. Critically, different additives yield suppression breakdown at different potential and, thus, broader or narrower hysteretic potential ranges; those providing broader hysteresis enable deposition at more negative potentials and thus the possibility of faster filling. However, although the exact details of the deposition depend on multiple factors, at the more negative potentials enabled by greater suppression, metal ion depletion within taller and narrower blind features such as TSV transforms deposition in experiments and associated S-NDR models from bottom-up filling to a passive-active transition down the sidewalls[12,13,64]. This study sought to maintain conditions consistent with the latter evolution as those processes also provide controlled self-passivation of filling in TSV. Low additive concentrations were therefore used. As seen, the desired control and self-passivation was obtained; although it was obtained at the cost of longer filling times the optimal conditions for robust and efficient filling remain to be determined.

Values of V_{Dep} toward the positive end of the hysteretic range exhibited deposition constrained to the via interiors with filling progressively more constrained at more positive

potentials (**Figure 7**); there was no evidence of active filling at a deposition potential of -0.44 V, localized deposition was minimal at -0.46 V and filling was complete at -0.52 V. That some amount of active deposition was observed ≈ 30 mV positive of the voltammetric hysteretic range reflects decrease of the additive concentrations over the considerable depth of the vias, i.e., a thicker transport boundary layer within the TGV relative to the smooth Cu RDE used in the voltametric survey experiments. The activation potential V_{Act} was selected to drive the workpiece negative of the suppression breakdown potential, observed at -0.60 V in the voltammetry. For deposition at V_{Dep} of -0.52 V it is observed that the activation at V_{Act} also exerts a strong influence on the localization as revealed with the V_{Act} potentials from -0.62 V to -0.68 V examined in **Figure 9**. The current transients during the deposition step at -0.52 V exhibit a substantial increase during the transient decay immediately following the pulses at -0.65 V, which persists for only a few hours, and throughout each cycle and the process as a whole for pulsing at -0.68 V. Further study will be required to understand the contributions of the current transient decay and steady state terms to the active and passive components of the filling evolution and, for that matter, the impact of the pulse, and its duration, on the de-passivation reflected in that transient. However, the observed increase of metal deposition and fill height with overpotential appears to reflect, in no small part, deposition associated with the current decay during the ≈ 100 s period immediately following the activation pulses, reflecting the importance of re-passivation kinetics in defining the shape of the growth front.

It should be noted that the conical via geometry greatly facilitates void-free feature filling. Even conformal deposition would, after bridging at the waist of the via, allow for void-free filling through geometrical leveling given the canted sidewalls. However, the absence of deposition higher in the vias or on the field is a unique attribute of the suppressor-derived S-NDR system. Superconformal filling with increased localization can be achieved at more

positive potentials, but the associated price is a longer filling time. Optimization to reduce filling time is a topic of practical concern and the conical vias naturally offer more latitude for improvement compared to the filling of cylindrical vias in which void formation may occur more readily and for which void-free filling through geometrical leveling is not possible.

CONCLUSION

Filling of through glass vias for use as glass interposers has been demonstrated in an acid copper sulfate electrolyte containing dilute chloride and poloxamine suppressor additives. Cyclic voltammetry with a RDE was used to characterize suppressor breakdown and re-passivation through the hysteretic response associated with the S-NDR bifurcation into active and passive zones as well as the important role of ohmic losses in the control loop that collectively impact via filling. The present work shows the utility of a periodic asymmetric pulsed potential deposition process with a 1 s activation step at V_{Act} to a potential negative of the voltametric hysteretic range and 10 min deposition at V_{Dep} toward the positive end of the hysteretic range. Localized deposition and void-free filling were obtained with the uniformity across the substrates improved through further cycling. Deeper understanding will require examination of the relative contributions to feature filling of the short ≈ 100 s period of enhanced deposition and re-passivation that follows the activation pulse to the more negative potentials. However, the uniform filling obtained across groups of vias despite the potential- and time-dependent variations observed at early times has significant implications for practical utilization of a filling mechanism based on S-NDR critical systems that can exhibit extreme sensitivity to electrolyte composition, feature geometry and hydrodynamics.

ACKNOWLEDGEMENTS

Certain equipment, instruments, software, or materials are identified in this paper in order to specify the experimental procedure adequately. Such identification is not intended to imply recommendation or endorsement of any product or service by the National Institute of Standards and Technology, nor is it intended to imply that the materials or equipment identified are necessarily the best available for the purpose. This work was supported by the Korea-US Joint Technology Development: "Development of electrically/mechanically reliable TGV technology for Next Generation of 3D Glass Via Interposer" (Project No. P0026243), funded by the Korea Institute for Advancement of Technology) (KIAT) grant funded by the Ministry of Trade, Industry and Energy (MOTIE), Republic of Korea.

REFERENCES

1. P. C. Andricacos, C. Uzoh, J. O. Dukovic, J. Horkans and H. Deligianni, *IBM J. Res. & Dev.*, **42**, 567 (1998).

2. T. P. Moffat, D. Wheeler and D. Josell, *Interface*, **13**, 46 (2004).

3. T. P Moffat, D. Raciti, T. M. Braun and D. Josell, *Acc. Chem. Res.* **56**, 1004 (2023).

4. J. P. Gambino, S. A. Adderly and J. U. Knickerbocker, *Microelectron. Engin.*, **135**, 73 (2015).

5. T. P. Moffat and D. Josell, *J. Electrochem. Soc*., **159**, D208 (2012).

6. D. Josell, D. Wheeler and T. P. Moffat, *J. Electrochem. Soc.*, **159**, D570 (2012).

7. D. Wheeler, T. P. Moffat and D. Josell, *J. Electrochem. Soc.*, **160**, D3260 (2013).

8. L. Yang, A. Radisic, J. Deconinck and P. M. Vereecken, *J. Electrochem. Soc.*, **160**, D3051 (2013).

9. M. Lefebvre, G. Allardyce, M. Seita, H. Tsuchida, M. Kusaka and S. Hayashi, *Circuit World*,

29, 9 (2003).

10. R. Tenno and A. Pohjoranta, *J. Electrochem. Soc.*, **155**, D383 (2008).

11. L. A. Min, D. Josell, T. P. Moffat, E. Baca, M. G. Blain, A. Smith, J. Dominguez, J. McClain, P. D. Yeh and A. E. Hollowell, *J. Electrochem. Soc.*, **166**, D3066 (2018).

12. D. Josell, L. A. Menck, A. E. Hollowell, M. Blain and T. P. Moffat, *J. Electrochem. Soc.*, **166**, D3254 (2019).

13. T. M. Braun, D. Josell, S. Deshpande, J. John and T. P. Moffat, *J. Electrochem. Soc.*, **167**, 162508 (2020).

14. J. Lee, Y. Kim, H. Han, S. Yoon, J-H Lim and B. Yoo, *ECS J. Solid State Sci. Tech.,* **12**, 114004 (2025). DOI: 10.1149/2162-8777/ad0872

15. W. P. Dow, H. H. Chen, M. Y. Yen, W. H. Chen, K. H. Hsu, P. Y. Chuang, H. Ishizuka, N. Sakagawa and R. Kimizuka, *J. Electrochem. Soc.*, **155**, D750 (2008).

16. W. P. Dow, D. H. Liu, C. W. Lu, C. H. Chen, J. J. Yan, and S. M. Huang, *Electrochem. Solid State Lett.*, **14**, D13 (2011).

17. G. Y. Lin, J. J. Yan, M. Y. Yen, W. P. Dow, and S. M. Huang, *J. Electrochem. Soc.*, **160**, D3028 (2013).

18.S. Shi, X. Wang, C. Xu, J. Yuan, J. Fang, S. Liu, *Sensor and Actuators A: Physical*, **203**, 52 (2013).

19. F. -Y. Shen, W. -P. Dow, A. -H. Liu, J. -Y. Lin, P. -H. Chang, S. -M. Huang, *ECS Electrochem. Lett.*, **2**, D23, (2013).

20. P. Ogutu, E. Fey, N. Dimitrov, *J. Electrochem. Soc.*, **162**, D457 (2015).

21. E. Fey, J. Li and N. Dimitrov, *J. Electrochem. Soc.*, **164**, D289 (2017).

22. Y. -H. Chang, P. -L. Tsent, J. -C. Lin, J. -C. Chen, M. -C. Huang, H. -Y. Lin, S. Pollard and P. Mazumder, *J. Electrochem. Soc.*, **166**, D3155 (2019).

24. T. M. Braun, D. Josell, J. John and T. P. Moffat, *J. Electrochem. Soc.,* **167**, 013510 (2020).

24. T. M. Braun, D. Josell, S. Deshpande, J. John and T. P. Moffat, *Electrochem. Soc.*, **167**, 162508 (2020).

25. S. Jayaraman, M. Sevem, R. Vaddi, M. Kanungo and P. Mazumder, *Electrochem. Comm.,* **120**, 106823 (2020).

26. T. M. Braun, D. Josell and T. P. Moffat, *Electrochim. Acta*, **375**, 137925 (2021).

27. T. M. Braun, J. John, N. Jayaraju, D. Josell and T. P. Moffat, *J. Electrochem. Soc.*, **169**, 012502 (2022).

28. F. Yang, Q. Wang, J. Lee, Y. Song, I. Hwang, S. Yoon and B. Yoo, *Surf. Interfaces*, **55**, 105431 (2024).

29. Y. -H. Chang, Y. -M. Lin, C. -Y. Lee, P. -C. Hsu, C. -M. Chen and C. -E. Ho, *J. Mater. Res. Tech.*, **31**, 1008 (2024).

30.C. Liang, Y. Chen, Y. Guo, W. Wu, M. Hou, H. Liu, L. Ma, X. Chen and C. Wong, *IEEE Transaction on Components*, *Packaging and Manufacturing Technology*, **15**, 1117 (2025).

31. Z. Yu, Y. Gao, X. Lei, Y. Chen, K. Xu, Y. Zshou and F. Zhu, *Electrochim. Acta*, **533**, 146556 (2025).

32. B. C. Baker, M. Freeman, B. Melnick, D. Wheeler, D. Josell and T. P. Moffat, *J. Electrochem. Soc.*, **150**, C61 (2003).

33. D. Josell and T. P. Moffat, *J. Electrochem. Soc.*, **160**, D3009 (2013).

34. D. Josell and T. P. Moffat, *Acc. Chem. Res*., **56**, 677 (2023).

35. C. H. Lee, J. E. Bonevich, J. E. Davies and T. P. Moffat, *J. Electrochem. Soc.*, **156**, D301 (2009).

36. D. Josell, M. Silva and T. P. Moffat, *J. Electrochem. Soc.*, **163**, D809 (2016).

37. J. Wu, F. Wafula, S. Branagan, H. Suzuki and J. van Eisden, *J. Electrochem. Soc.*, **166**,

D3136 (2019).

38. M. A. Rigsby, L. J. Brogan, N. V. Doubina, Y. Liu, E. C. Opocensky, T. A. Spurlin, J. Zhou and J. D. Reid, *J. Electrochem. Soc.*, **166**, D3167 (2019).

39. S. -K Kim, J. E. Bonevich, D. Josell and T. P. Moffat, *J. Electrochem. Soc.*, **154**, D443 (2007).

40. D. Josell and T. P. Moffat, *J. Electrochem. Soc.*, **163**, D322 (2016).

41. T.P. Moffat, D. Wheeler and D. Josell, "Superconformal Film Growth," in Advances in Electrochemistry and Electrochemical Engineering, Vol. 10., pp. 107-189, eds. R.C. Alkire, D.M. Kolb, P. Ross and J. Lipkowski, Wiley-VCH, (2008) and references therein.

42. S. -H. Kim, H. -J. Lee, D. Josell and T. P. Moffat, *Electrochim. Acta*, **335**, 135612 (2020).

43. S. -H. Kim, H. -J. Lee, T. M. Braun, T. P. Moffat and D. Josell, *J. Electrochem. Soc.*, **168**, 112501 (2021).

44. S. -H. Kim, T. M. Braun, H. -J. Lee, T. P. Moffat and D. Josell, *J. Electrochem. Soc.*, **169**, 032508 (2022).

45. V. Grimaudo, P. Moreno-Garcia, A. C. Lopez, A. Riedo, R. Wiesendanger, M. Tulej, C. Gruber, E. Lortscher, P. Wurz and P. Broekmann, *Anal. Chem.*, **90**, 5179 (2018).

46. A. Chrzanowska and R. Mroczka, *Electrochim. Acta*, **78**, 316 (2012).

47. Z. Nagy, J. P. Blaudeau, N. C. Hung, L. A. Curtiss and D. J. Zurawski, *J. Electrochem. Soc.*, **142**, L87 (1995).

48. T. P. Moffat, STM Studies of Halide Adsorption on Cu(100), Cu(110) and Cu(111). *Electrochemical Processing in ULSI Fabrication and Semiconductor/Metal Deposition II*, Electrochemical Society Proceeding 1999, Vol. 99-9, pp. 41-51, Eds. P. C. Andricacos, P. C. Searson, C. Reidsema-Simpson, P. Allongue, J. L. Stickney, G. M. Oleszek (The Electrochemical Society, 2018).

49. Y. Grunder, A. Drunkler, F. Golks, G. Wijts, J. Stettner, J. Zegenhagen and O. M. Magnussen, *Surf. Sci.*, **605**, 1732 (2011).

50. K. Wandelt, Interaction of Chloride Anions with Copper Surfaces, *Encyclopedia of Interfacial Chemistry: Surface Science and Electrochemistry*, pp. 166-181, Ed. K. Wandelt, (Elsevier, 2018).

51. M. R. H. Hill and G. T. J. Rogers, *J. Electroanal. Chem.*, **86**, 179 (1978).

52. K. Doblhofer, S. Wasle, M. Soares, K. G. Weil and G. Ertl, *J. Electrochem. Soc.*, **150**, C657 (2003).

53. M. L. Walker, L. J. Richter and T. P. Moffat, *J. Electrochem. Soc.*, **152**, C403 (2005).

54. K. R. Hebert, *J. Electrochem. Soc.,* **152**, C283 (2005).

55. D. Brazinskiene and A. Survila, *Russian J. Electrochem.*, **41**, 979 (2005).

56. J. G. Long, P. C. Searson and P. M. Vereecken*J. Electrochem. Soc.*, **153**, C258 (2006).

57. R. T. Rooney, K. G. Schmitt, H. F. Von Horsten, R. Schmidt and A. A. Gewirth, *J. Electrochem. Soc.*, **165**, D687 (2018).

58. G.-K. Liu, S. Zou, D. Josell, L. J. Richter and T. P. Moffat, *J. Phys. Chem. C.*, **122**, 21933 (2018).

59. R. Schmidt, J. M. Knaup and H. F. von Horsten, *Advanced Theory and Simulations*, **3**, 1900160 (2020).

60. M. Hayase, M. Taketani, K. Aizawa, T. Hatsuzawa and K. Hayabusa, *Electrochem. Solid-State Lett.,* **2002**, *5*, C98-C101.

61. J. W. Gallaway and A. C. West, *J. Electrochem. Soc.*, **155**, D632 (2008).

62. L. Yang, A. Radisic, J. Deconinck, P. M. Vereecken, *J. Electrochem. Soc.,* **161**, D269 (2014).

63. H. Yang, A. Dianat, M. Bobeth and G Cuniberti, *J. Electrochem. Soc.,* **164**, D196 (2017).

64. D. Josell and T. M. Moffat, *J. Electrochem. Soc.*, **165**, D23 (2018).

65. T. M. Braun, D. Josell, M. Silva, J. Kildon and T. P. Moffat, *J. Electrochem. Soc.*, **166**, D3259 (2019).

66. N. T. M. Hai, T. M. T. Huynh, A. Fluegel, D. Mayer and P. Broekmann, *Electrochimica Acta*, **56**, 7361 (2011).

67. N. T. M. Hai, J. Furrer, F. Stricker, T. M. T. Huynh, I. Gjuroski, N. Luedi, T. Brunner, F. Weiss, A. Fluegel, M. Arnold, I. Chang, D. Mayer and P. Broekmann, *J. Electrochem. Soc.*, **160**, D3116 (2013).

68. Y. -J. Li, J. Oslonovitch, N. Mazouz, F. Plenge, K. Krischer and G. Ertl, *Science*, **291**, 2395 (2001).

69. K. Krischer, Nonlinear dynamics in electrochemical systems in *Advances in Electrochemical Science and Engineering Vol. 8*. Editors: R. C. Alkire and D. M. Kolb. pp. 89-208 (2003).

70. B. K. Wang, Y. -A. Chen, A. Shorey and G. Piech, "Thin Glass substrates development and integration for through glass vias (TGV) with copper (Cu) interconnects", in *2012 7th International Microsystems, Packaging, Assembly and Circuits Technology Conference (IMPACT)* pp. 247 - 250 (IEEE). DOI: 10.1109/IMPACT.2012.6420306

71. J. Liu, C. Xia, X. Ming, G. Dou and C. Yin, *Adv. Engin. Mater.*, **26**, 2400397 (2024). DOI: 10.1002/adem.202400397

72. P. Nimbalkar, P. Bhaskar, L. N. V. Kumar, M. Narayanan, E. Torres, S. S. A. Venkataramanan and M. Kathaperumal, *Chips*, **4**, 37 (2025); DOI: 10.3390/chips4030037

73. X. Zhang X. Wang, Y. Li, J. Huang, Y. Wang, L. Xing, S. Liu, W. Yang, J. Zhang, H. Hong, Y. Tian, H. Luo, R. Wang, *ACS Appl. Electron. Mater*., **7**, 10822 (2025).

74. A. Usman, E. Shah, N. B. Satishprasad, J. Chen, S. A. Bohlemann, S. H. Shami, A. A. Eftekhar, A. Adibi, *IEEE Transactions on Components, Packaging and Manufacturing*

Technology, **7**, 819 (2017).

75. V. Sukumaran, T. Bandyopadhyay, V. Sundaram and R. Tummala, *Transactions on Component, Packaging and Manufacturing Technology*, **2**, 1426 (2012).

76. S. M. George, *Chem. Rev.*, **110**, 111 (2010). DOI: 10.1021/cr900056b

77. S. Wolf, M. Breeden, I. Kwak, J. H. Park, M. Kavrik, M. Naik, D. Alvarez, J. Spiegelman and A. C. Kummel, *Appl. Surf. Sci.*, **462**, 1029 (2018). DOI: 10.1016/j.apsusc.2018.07.153

78. E. -L. Lokomaa, S. Haukka and T. Suntola, *Appl. Surf. Sci.*, **60-61**, 742 (1992).

79. J. -Y. Kim, D. -S. Kil, J. -H. Kim, S. -H. Kwon, J. -H. Ahn, J. -S. Roh and S. -K. Park, *J. Electrochem. Soc.*, **159**, H560 (2012).

80. J. Lu and J. W. Elam, *Chem. Mater.*, **27**, 4950 (2015).

81. M. Mattinen, J. Hämäläinen, M. Vehkamäki, M. J. Heikkilä, K. Mizohata, P. Jalkanen, J. Räisänen, M. Ritala and M. Leskelä, *J. Phys. Chem. C*, **120**, 15235 (2016).

82. T. P. Moffat, M. Walker, P. J., Chen, J. E. Bonevich, W. F. Egelhoff, L. Richter, C. Witt, T. Aaltonen, M. Ritala, M. Leskela and D. Josell, *J. Electrochem. Soc.*, **153**, C37 (2006).

83. M. Walker, L. Richter, D. Josell and T. P. Moffat, *J. Electrochem. Soc.*, **153**, C235 (2006).